ACS OMEGA

http://pubs.acs.org/journal/acsodf

Article

Mechanochemically Synthesized Prussian Blue for Efficient Removal of Cesium Ions from Aqueous Solutions

Ji Hwan Lee and Seung-Yeop Kwak*

Cite This: *ACS Omega* 2022, 7, 3222−3229

Read Online

ACCESS | Metrics & More | Article Recommendations | Supporting Information

ABSTRACT: The adsorptive removal of radioactive cesium [Cs(I)] is important for ensuring a clean aquatic environment. In this work, the adsorption of Cs(I) was carried out using Prussian blue (PB) prepared by mechanochemical synthesis. X-ray diffraction, Fourier-transform infrared spectroscopy, and field-emission scanning electron microscopy results indicated that PB had been successfully synthesized by mechanochemical synthesis. Thermogravimetric analysis, contact angle analysis, inductively coupled plasma atomic emission spectrometry, elemental analysis, and electrophoretic light scattering spectrophotometry confirmed that several defects were formed, explaining the principal mechanism for the efficient adsorption over PB prepared by mechanochemical synthesis. The superior adsorption properties toward Cs(I) make PB prepared by mechanochemical synthesis an attractive candidate material for the efficient, economical, and eco-friendly processes for purifying radioactive wastewater.

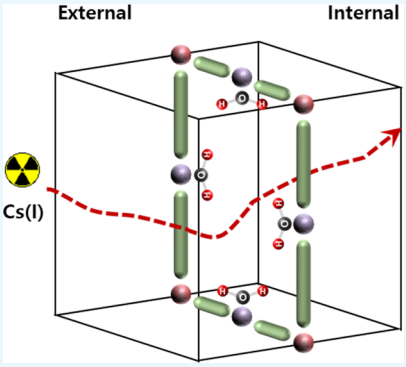

1. INTRODUCTION

Past nuclear accidents such as the Chernobyl accident and the Fukushima accident have reminded us of the long-term and catastrophic disaster resulted from the discharge of radioactive species. Among the radioactive species, the cesium isotope ^{137}Cs(I) is a major species in radioactive liquid waste because it has a long half-life while emitting high-energy gamma rays and can be easily incorporated in the living organisms due to their chemical similarity to potassium, resulting in a serious radiological hazard.[1] Thus, it is urged to selectively remove Cs(I) from radioactive liquid waste.[2]

Adsorption is considered to be an efficient and simple approach for the removal of the radioactive species such as Cs(I).[3] The dark-blue pigment Prussian blue (PB), a member of the metal−organic frameworks (MOFs), can bind hazardous substances such as Cs(I), Tl(I), and organophosphorus pesticides in an aqueous environment.[4,5] PB can be categorized into two types: insoluble PB ($Fe(III)_4[Fe(II)(CN)_6]_3{\cdot}xH_2O$; IPB) and soluble PB ($M(I)Fe(III)[Fe(II)(CN)_6]$; SPB).[6,7] The main adsorption mechanism is known to be the exchange of cations within the SPB structure with Cs(I).[8,9] Adsorption by IPB can be explained by the exchange of protons eliminated from a coordination water in a lattice defect site for Cs(I) because it has no interstitial cations in the lattice structure unlike SPB.[10] Other mechanisms include percolation of Cs(I) with a dehydrated state through lattice defect sites from the surface of PB.[11] In general, IPB exhibits more advantages for the adsorption process because it is easier to recover IPB from aqueous solutions after the adsorption process.[12] PB has been widely used as the main ingredient of the drug, Radiogardase, which is approved for the treatment of radioactive cesium poisoning due to safety and non-toxicity for both humans and the environment.[13,14] However, the majority of PBs have been prepared by solution-based synthesis such as co-precipitation, emulsion, sonochemical, hydrothermal, and microwave-assisted methods, which require high energy consumption, long reaction times, use of solvents, or additives such as a surfactant and an acid.[7] These requirements may result in a low productivity of PB and create issues with environmental pollutant effluents.

To improve the adsorptive properties of PB, we have applied the concept of "defect control" in MOF research, which focuses on fine-tuning the physical, structural, and chemical properties of MOFs. Various synthesis parameters for MOFs have been adjusted to control defects, such as coordinatively unsaturated sites (CUSs), which only partially coordinate with the organic linkers. For instance, Canivet *et al.* proposed that high reaction rates result in the formation of defects while maintaining the original MOF structure.[15] It has also been reported that the generated defects improve the adsorptive properties of MOFs by providing additional interaction locations.[16,17]

Mechanochemical synthesis, an alternative synthesis method that induces chemical reactions through the input of mechanical energy without a solvent, exhibits advantages

Received: September 13, 2021
Accepted: January 5, 2022
Published: January 19, 2022

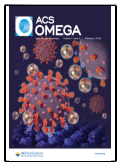

https://doi.org/10.1021/acsomega.1c05062
ACS Omega 2022, 7, 3222−3229

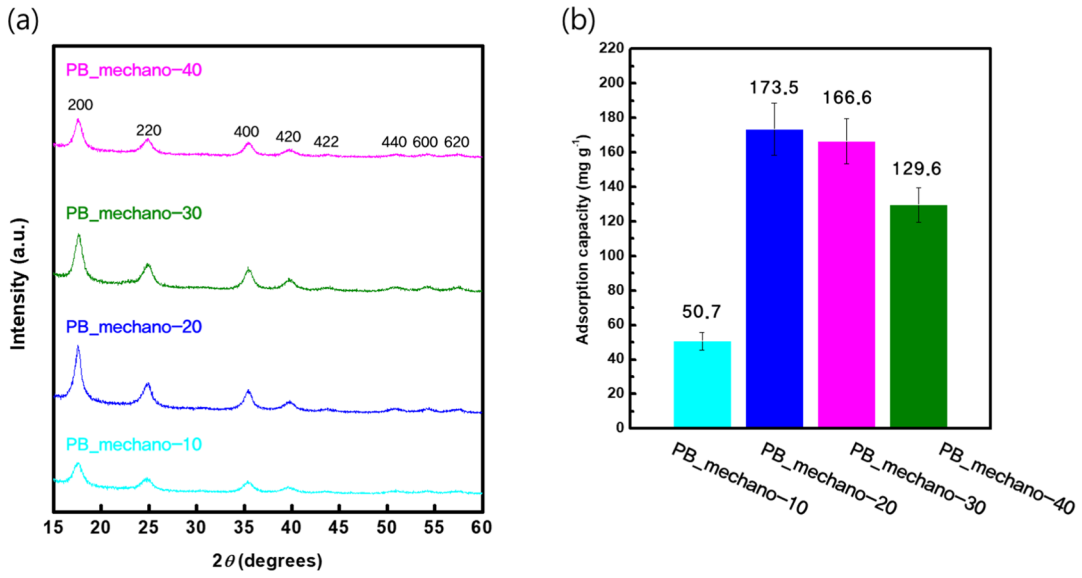

Figure 1. (a) XRD patterns and (b) adsorption capacities of PB_mechano samples.

over conventional solution-based syntheses such as higher reaction rates, lower reaction temperatures, cost-effectiveness, and eco-friendliness.[18] It is therefore considered a facile and eco-friendly synthesis method for inorganic frameworks, organic frameworks, and MOFs.[19,20] We hypothesize that mechanochemical synthesis could generate defects more effectively than conventional synthesis due to the increased reaction rate, thereby enhancing the adsorptive properties of PB.

To the best of our knowledge, we are the first to develop PB by mechanochemical synthesis, henceforth denoted as PB_mechano, for the selective removal of Cs(I) from aqueous solutions. The readily synthesized PB_mechano without a solvent exhibited superior adsorptive properties (1260 mg g^{-1}) to commercial PB despite its lower specific surface area (0.5 m^2 g^{-1}) and more positive zeta potential (−22.4 mV) because mechanochemical synthesis more efficiently produces defects and lattice strain (0.00857) in the framework than conventional synthesis. PB_mechano offers the possibility of developing efficient, economical, and eco-friendly processes for the removal of radionuclides from radioactive wastewater.

2. MATERIALS AND METHODS

2.1. Materials. Potassium hexacyanoferrate(III), iron(II) chloride tetrahydrate, cesium (^{133}Cs) chloride, and commercial PB were purchased from Sigma-Aldrich. Since the chemical properties of the radionuclide are identical to its stable isotope, the stable isotope of cesium (^{133}Cs) was used for experiments. The water used in all experiments was deionized (DI).

2.2. Mechanochemical Synthesis of PB. PB_mechano was prepared by a solvent-free mechanochemical method. Potassium hexacyanoferrate(III) and iron(II) chloride tetrahydrate (molar ratio 3:4) were mixed by grinding in an agate mortar for various times t (min) at room temperature. The product, referred to as PB_mechano-t, was sequentially washed with DI water and then vacuum-dried at room temperature overnight.

2.3. Characterization. X-ray diffraction (XRD) patterns were recorded with a New D8 ADVANCE X-ray diffractometer (Bruker, USA) using Cu Kα radiation. Fourier-transform infrared (FT-IR) spectra were acquired using a Nicolet iS10 IR spectrophotometer (Thermo Fisher Scientific, USA) with the samples in potassium bromide pellet form. Thermogravimetric analysis (TGA) was conducted using a Q500 system (TA Instruments, USA), and static pure water contact angle was examined with an Attention THETA LITE contact angle meter (Biolin Scientific, Sweden). Color analysis was conducted using a V-770 ultraviolet−visible (UV−vis) spectrophotometer (JASCO, USA). The samples were then scanned for reflectance ranging from 200 to 800 nm. Field-emission scanning electron microscopy (FE-SEM) images were obtained using a SUPRA 55VP field-emission scanning electron microscope (Zeiss, Germany). High-resolution transmission electron microscopy (HR-TEM) was performed using a JEM-F200 (JEOL, Japan) microscope operated at an accelerating voltage of 200 kV. Nitrogen adsorption−desorption isotherms were obtained using a 3Flex surface characterization analyzer (Micromeritics, USA), and the zeta potential was evaluated using a Z-1000 electrophoretic light scattering (ELS) spectrophotometer (Otsuka Electronics, Japan). Inductively coupled plasma mass spectrometry (ICP−MS) measurements were performed with a NexION 350D (PerkinElmer, USA). The chemical composition was determined using elemental analysis (EA) and inductively coupled plasma atomic emission spectrometry (ICP−AES) measurements. EA was performed using a Flash EA 1112 analyzer (Thermo Fisher Scientific, USA). ICP−AES was performed using an OPTIMA 8300 analyzer (PerkinElmer, USA).

2.4. Batch Adsorption Experiments. The adsorption measurement was conducted in aqueous solutions with various initial cesium concentrations of 6.25−800 mg L^{-1}. PB (2 mg) was added to a cesium aqueous solution (10 mL) at a specific pH (usually 5.6) and then stirred at 25 °C. The residual concentrations of cesium in solution were determined by ICP−MS.

The models used to explain the adsorption kinetics of Cs(I) on PB included the pseudo-first-order (PFO) and pseudo-second-order (PSO) models. The two kinetic equations are as follows

$$q_t = q_e(1 - e^{-k_1 t}) \quad (1)$$

https://doi.org/10.1021/acsomega.1c05062
ACS Omega 2022, 7, 3222−3229

$$q_t = \frac{q_e^2 k_2 t}{1 + k_2 q_e t} \quad (2)$$

where q_t (mg g^{-1}) is the adsorption capacity of PB at time t and k_1 (min^{-1}) and k_2 (g mg^{-1} min^{-1}) are the PFO rate constant and the PSO rate constant, respectively.

The models used to explain the adsorption isotherms of Cs(I) on PB included the Freundlich and Langmuir isotherm models. The two isotherm equations are as follows

$$q_e = K_F C_e^{1/n} \quad (3)$$

$$q_e = \frac{q_L K_L C_e}{1 + K_L C_e} \quad (4)$$

where K_F ((mg g^{-1}) (L $mg^{-1})^n$) is the Freundlich constant, n (unitless) is the heterogeneity factor, K_L (L mg^{-1}) is the Langmuir constant, and q_L (mg g^{-1}) is the maximum adsorption capacity of PB.

All experiments were performed in triplicate.

3. RESULTS AND DISCUSSION

3.1. Optimal Conditions to Prepare PB_mechano. The XRD patterns were analyzed to determine the crystalline structures of the PB_mechano samples. As shown in Figure 1a, all PB_mechano samples showed the characteristic peaks of PB attributed to the (200), (220), (400), (420), (422), (440), (600), and (620) planes.[21]

Table 1. XRD Results of PB_mechano Samples

sample	*h k l*	*d*-spacing (nm)	crystallite size (nm)
PB_mechano-10	2 0 0	0.50	7.64
PB_mechano-20	2 0 0	0.51	11.59
PB_mechano-30	2 0 0	0.50	8.43
PB_mechano-40	2 0 0	0.50	8.65

The adsorption capacities of the PB_mechano samples were measured to verify the optimal preparation conditions for superior adsorptive properties. The adsorption measurements were conducted for 840 min in a solution with an initial Cs(I) concentration of 100 mg L^{-1}. PB_mechano-20 had the highest adsorption capacity for Cs(I) (Figure 1b). Based on these results, PB_mechano-20 was employed in further analyses to document its structural properties and adsorption behavior.

Based on the XRD analyses by Bragg's diffraction equation and Debye−Scherrer equation in Table 1, we hypothesize that if the grinding time is too short, PB_mechano does not have a PB crystal structure (*d*-spacing away from 0.51 nm, the characteristic *d*-spacing of PB and small crystallite size), so the cesium adsorption capacity is low. If mechanochemical grinding proceeds too much, the crystal structure of PB will collapse due to mechanical collision and abrasion, resulting in the low cesium adsorption capacity. Therefore, we consider that 20 min is enough time to build a PB structure.

3.2. Comparison of PB_mechano and Commercial PB. As shown in Figure 2a, the crystalline structures of PB_mechano and commercial PB were compared by XRD analysis. The commercial PB exhibited the same cubic crystal structure as PB_mechano as indicated by the XRD peaks in the same 2θ positions. However, each XRD signal of commercial PB was sharper than that of PB_mechano. The average crystallite size and lattice strain of PB_mechano and commercial PB were estimated according to the Williamson−Hall method (Table 2, Figure S1a).[6,22] The lattice strain induced in PB_mechano might be attributed to crystal imperfection and distortion resulted from the defect sites. The lattice constants of PB_mechano and commercial PB were also calculated as 1.015 and 1.020 nm, respectively, by the extrapolation method using the Nelson−Riley function (Table 2, Figure S1b).[12] These lattice constants are consistent with the characteristic unit length of Fe(II)−CN−Fe(III) in the PB structure. The photo images and visible reflectance spectra of PB_mechano and commercial PB are shown in Figure S2. The color coordinates of PB_mechano and commercial PB were also calculated from the measured reflectance spectra and are listed in Table S1. The color of PB_mechano and commercial PB is blue, and there is no significant difference as a result of color analysis. In Figure 3, the morphologies of PB_mechano and commercial PB were investigated using FE-SEM and HR-TEM. The FE-SEM and HR-TEM images showed that both PB_mechano and commercial PB had spherical morphologies with sizes of *ca.* 20 and 70 nm, respectively. The smaller crystallite size and particle size of PB_mechano might be due to insufficient crystallization resulting from the reduced reaction time.[23]

The PB FT-IR spectra shown in Figure 2b contain IR bands characteristic of the PB structure. The IR bands at ∼3400 and ∼1600 cm^{-1} are associated with the O−H stretching and bending vibrations, respectively.[24] These IR bands of water molecules in PB_mechano are stronger than those of commercial PB, indicating that PB_mechano included more water molecules in its structure. The characteristic bands at 2078, 600, and 500 cm^{-1} correspond to the CN stretching, Fe(II)−CN bending, and CN−Fe(III) bending vibrations, respectively.[25] These vibrational bands indicated that the cyan molecules were linked to the iron clusters. Additional IR bands in the commercial PB spectrum at 3260 and 1415 cm^{-1} implied the existence of ammonium ions [NH_4(I)] as cations in the cubic structure (Figure 2b).

The TGA profiles of PB_mechano and commercial PB, given in Figure 2c, showed an initial weight loss below 200 °C (11.0 and 5.9%, respectively) corresponding to the loss of water molecules from the structure of PB. The second weight loss above 200 °C (36.0 and 40.1%, respectively) arises from the collapse of the PB structure due to the thermal decomposition of the structural CN binding. Ludi *et al.* reported that the water molecules of PB correspond to coordination or crystallization water molecules.[26] The larger weight loss in PB_mechano than that in commercial PB indicates that PB_mechano had a large number of coordination or crystallization water molecules and, thus, that PB_mechano might be more hydrophilic than commercial PB. The static pure water contact angles were also examined to quantitatively evaluate the hydrophilicity of PB (Figure 2d). The lower contact angle of PB_mechano indicated that PB_mechano was more hydrophilic than commercial PB. Zakaria and Chikyow reported that interstitial water molecules existed in the framework of IPB and caused some defects.[7] Ishizaki *et al.* concluded that the lattice defect sites (vacant sites of [$Fe(CN)_6$]) of IPB were filled with coordination or crystallization water molecules, which caused the formation of hydrophilic spaces in the PB structure.[10] These results suggested that PB_mechano was IPB and commercial PB was SPB. The chemical compositions of the samples were actually evaluated through the results of EA and ICP−AES

https://doi.org/10.1021/acsomega.1c05062
ACS Omega 2022, 7, 3222−3229

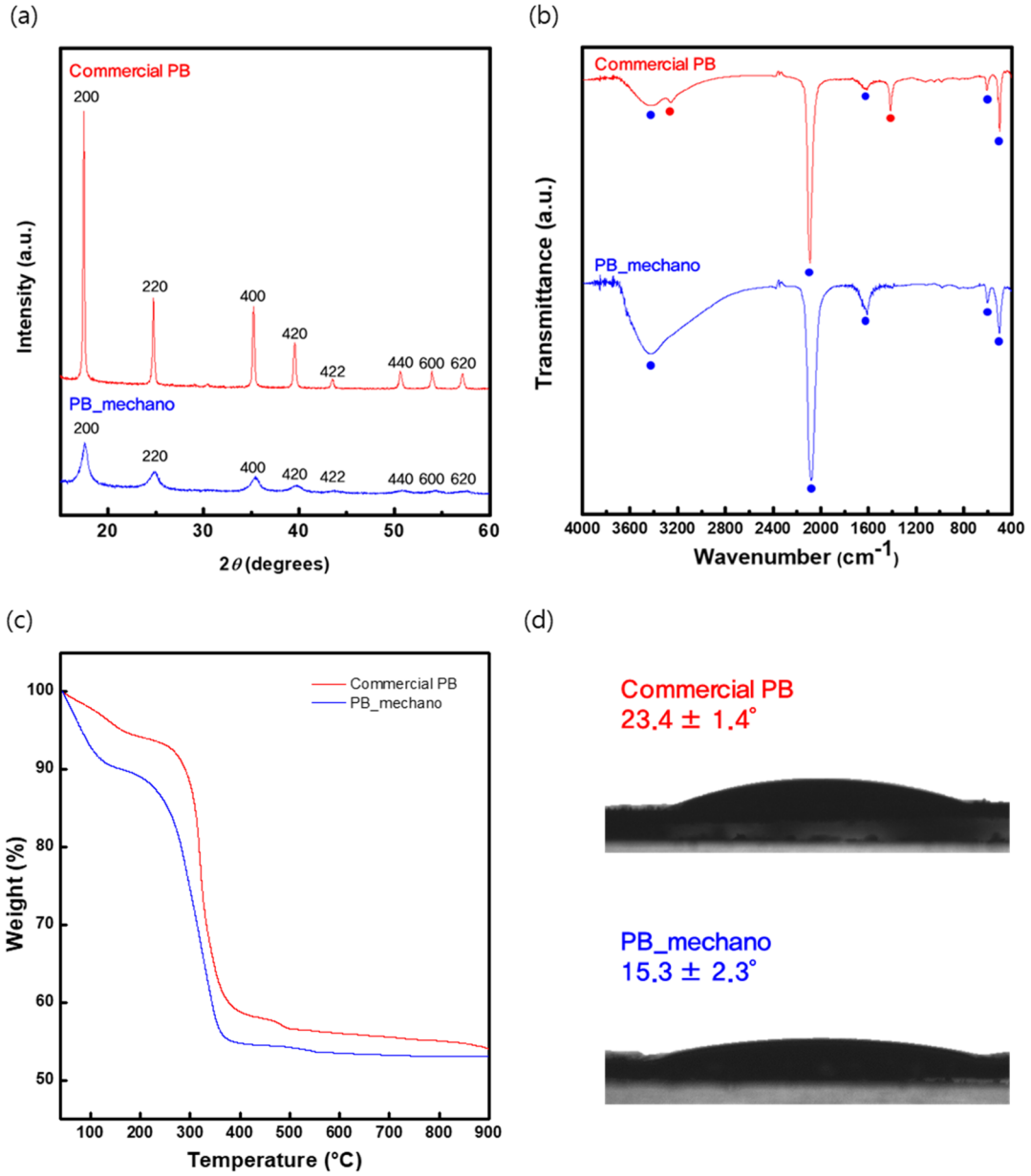

Figure 2. (a) XRD signals, (b) FT-IR spectra, (c) TGA profiles, and (d) static pure water contact angles of commercial PB and PB_mechano.

Table 2. XRD Results of Commercial PB and PB_mechano

sample	average crystallite size (nm)	lattice constant (nm)	lattice strain
commercial PB	41.69	1.020	0
PB_mechano	11.59	1.015	0.00857

using this simple principle of electrical neutrality and are listed in Table 3. The charge balance of chemical composition was satisfied by hydroxyl ions to which some water molecules in the composition were converted.[11] The EA results also reflected that NH_4(I) existed in commercial PB, indicating that commercial PB was SPB, which included NH_4(I) as the charge compensation cation. The estimated chemical composition of commercial PB was well coincident with general chemical composition of SPB ($M_{1-4\alpha}Fe[Fe(CN)_6]_{1-\alpha}V_\alpha$ (α: 0−0.25), where V is the $[Fe(CN)_6]$ vacancy site),[22] indicating that commercial PB included few vacancy sites due to the small α value (*ca.* 0.11). However, PB_mechano was found to include a lower amount of $[Fe(CN)_6]$ and a higher amount of water molecules than commercial PB because PB_mechano was IPB, in which Fe(II) was in excess of Fe(III) $(CN)_6$ in the synthesis condition. The estimated chemical composition of PB_mechano showed that PB_mechano had less $[Fe(CN)_6]_3$ than general IPB ($Fe_4[Fe(CN)_6]_3V$, where V is the $[Fe(CN)_6]$ vacancy site). Therefore, these results suggested that PB_mechano included more defect sites than commercial PB.

3.3. Cesium Adsorption by PB_mechano and Commercial PB. Figure 4a illustrates the adsorption kinetics of Cs(I) by commercial PB and PB_mechano at C_0 (1000 mg L^{-1}) during the period from 0 to 840 min. Cs(I) adsorption rapidly increased and reached equilibrium after 10 min. The initial rapid adsorption was attributed to an instantaneous adsorption process arising from the many available vacant adsorption sites.[27] The kinetic parameters given in Table 4 indicate that Cs(I) adsorption can be explained with the PSO kinetic model according to the resulting correlation coef-

https://doi.org/10.1021/acsomega.1c05062
ACS Omega 2022, 7, 3222−3229

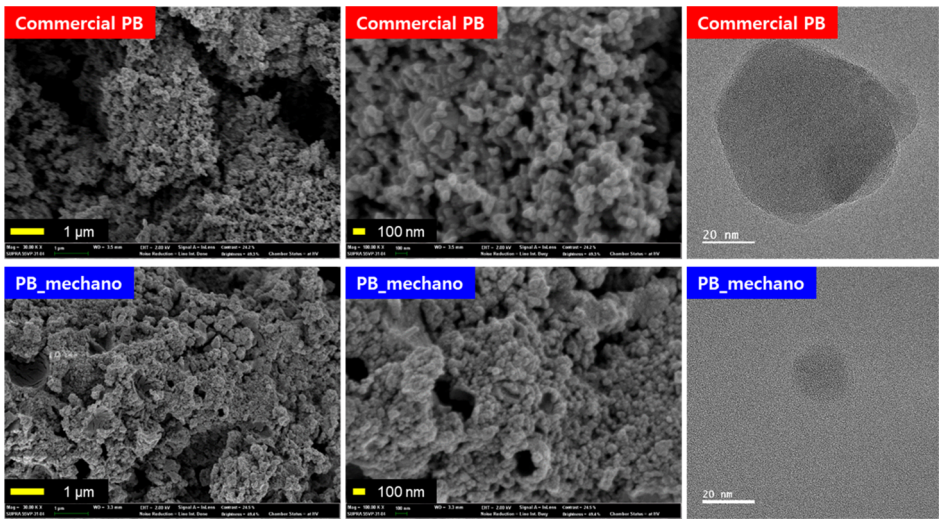

Figure 3. FE-SEM and HR-TEM images for commercial PB and PB_mechano.

Table 3. Chemical Compositions of Commercial PB and PB_mechano

sample	[a]Fe (wt %)	[b]N (wt %)	[b]C (wt %)	[b]H (wt %)	chemical composition
commercial PB	36.80	28.91	22.42	1.82	$(NH_4)_{0.57}Fe[Fe(CN)_6]_{0.89}\bullet 1.46H_2O$
PB_mechano	35.06	22.03	18.69	2.26	$Fe_4[Fe(CN)_6]_{2.80}\bullet 12.00H_2O$

[a]Value evaluated by ICP−AES. [b]Value evaluated by EA.

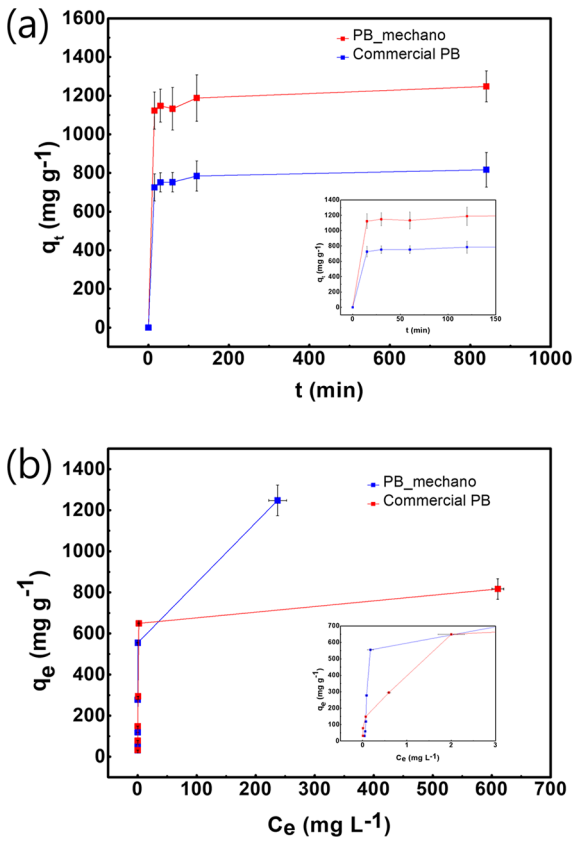

Figure 4. (a) Adsorption kinetics and (b) adsorption isotherms of commercial PB and PB_mechano for Cs(I).

ficients. PB_mechano exhibited a similar rate constant but a considerably higher equilibrium adsorption capacity than commercial PB.

Figure 4b shows the adsorption isotherms of Cs(I) by commercial PB and PB_mechano at various C_0 (800−6.25 mg L^{-1}) for 840 min. The isotherm parameters given in Table 5 indicate that the Langmuir model best described the adsorption of Cs(I) by PB_mechano and commercial PB. The type of adsorption (*i.e.*, irreversible, favorable, linear, or unfavorable) can be predicted using the separation factor R_L, defined by eq 5[28]

$$R_L = \frac{1}{1 + K_L C_0} \tag{5}$$

where K_L (L mg^{-1}) is the Langmuir constant and C_0 (mg L^{-1}) is the initial adsorbate concentration.

Depending on the R_L value, the adsorption can be classified as unfavorable ($R_L > 1$), linear ($R_L = 1$), favorable ($0 < R_L < 1$), or irreversible ($R_L = 0$). The R_L values for the adsorption of Cs(I) by PB_mechano and commercial PB showed that both samples adsorbed Cs(I) favorably. The Langmuir model also estimated that the maximum adsorption capacities of PB_mechano and commercial PB for Cs(I) were 1260.1 and 831.9 mg g^{-1}, respectively, although an inverse relationship was noted for the specific surface area and zeta potential. As shown in Figure S3, the nitrogen adsorption−desorption isotherms indicated that commercial PB (54.9 m^2 g^{-1}) had a specific surface area 100 times larger than that of PB_mechano (0.5 m^2 g^{-1}). Figure S3 shows that commercial PB has a surface charge of approximately −22.4 mV at a pH value of 5.6, which is consistent with the values reported previously.[29] This negative surface charge of commercial PB could lead to an electrostatic attraction between commercial PB and Cs(I). Figures S4 and S5 indicate that PB_mechano had a surface charge of approximately −5.9 mV at a pH value of 5.6, which is more positive than that of commercial PB; this suggests that mechanochemical synthesis generates positively charged CUSs as defects more effectively than conventional synthesis.

https://doi.org/10.1021/acsomega.1c05062
ACS Omega 2022, 7, 3222−3229

Table 4. Adsorption Kinetic Parameters for Cs(I)

adsorbent	PFO kinetic			PSO kinetic		
	q_e	k_1	R^2	q_e	k_2	R^2
commercial PB	778.0	0.1756	0.9932	797.7	0.0007	0.9973
PB_mechano	1180	0.1976	0.9915	1207	0.0006	0.9952

Table 5. Adsorption Isotherm Parameters for Cs(I)

adsorbent	Freundlich isotherm			Langmuir isotherm			
	K_F	n	R^2	q_L	K_L	R_L	R^2
commercial PB	380.0	7.9	0.8128	831.9	1.2859	0.0013−0.9999	0.9511
PB_mechano	376.0	4.5	0.8325	1260.1	2.7394	0.0015−0.8958	0.9373

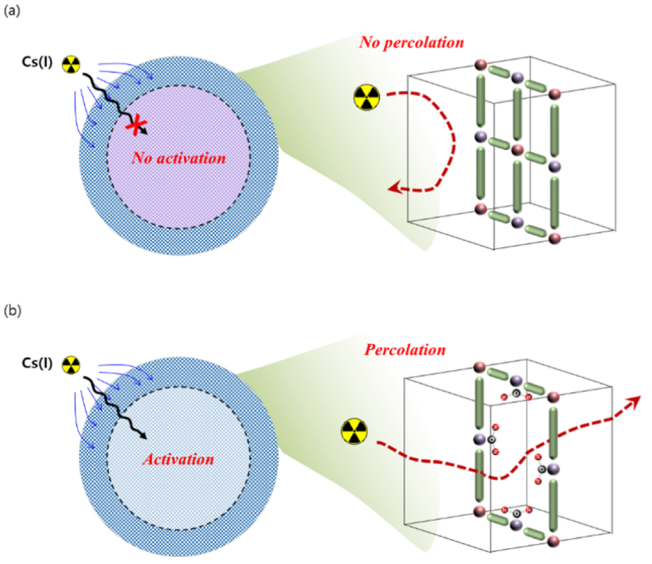

Figure 5. Proposed Cs(I) adsorption mechanisms of (a) commercial PB and (b) PB_mechano.

However, positively charged PB_mechano cannot efficiently induce an electrostatic attraction with Cs(I). In a study on potassium copper hexacyanoferrate (KCuHCF), a PB analogue, Takahashi *et al.* proposed a "percolation *via* vacancies" model wherein Cs(I) cannot migrate in the perfect lattice of KCuHCF but can migrate through $[Fe(CN)_6]$ vacancies.[11] It is reasonable to state that Cs(I) can not only be adsorbed on the surface of PB particles but can also penetrate and be adsorbed inside. Therefore, although commercial PB has a higher specific surface area and a more negative surface charge, the lower Cs(I) removal of commercial PB than that of PB_mechano can be explained by the fact that only surface adsorption occurs due to the highly crystalline structure (Figure 5a). Figure 5b illustrates that PB_mechano, in contrast, can capture Cs(I) over the entire structure *via* surface adsorption and percolation despite the lower specific surface area and more positive surface charge.

The maximum adsorption capacity and synthetic conditions of PB_mechano were compared with those in previous reports on PB-based adsorbents to confirm the potential of PB_mechano as an adsorbent for Cs(I).[10,14,24,25,30] As shown in Table 6, the maximum adsorption capacity of PB_mechano for Cs(I) is significantly higher than those of other previously studied adsorbents. Considering the sufficient adsorption capacity and simple preparation method of PB_mechano, it can be regarded as an efficient, economical, and eco-friendly adsorbent in the area of radioactive wastewater treatment.

4. CONCLUSIONS

In summary, PB_mechano was used to remove Cs(I) from aqueous solutions for the first time. The XRD, FT-IR, and FE-SEM results confirmed that PB was successfully synthesized by the mechanochemical approach. The TGA, contact angle analysis, EA, ICP−AES, and ELS revealed that many defects were formed by mechanochemical synthesis, which affected the interaction necessary for the adsorption of Cs(I) onto PB_mechano. The adsorption of Cs(I) onto PB_mechano followed the PSO kinetic model and Langmuir isotherm model with a superior adsorption capacity to that obtained using commercial PB. The superior adsorption properties toward Cs(I) make PB_mechano an attractive candidate material for

Table 6. Comparison of Maximum Adsorption Capacities and Synthetic Conditions of PB-Based Adsorbents

adsorbent	maximum adsorption capacity (mg g^{-1})	adsorbent mass/adsorption time/pH	synthetic condition	refs
CNF-backboned PB	139	n.a.	stirring at RT overnight, DI water	24
chitin-supported PB	42	0.1 g/48 h/pH 5−6	dropwise addition, stirring at RT for 30 min, DI water	25
PB nanoparticles	∼130	0.5 g/6 h/pH 2.5	stirring at RT for 15 min,DI water	10
PMMA-supported PB	20	0.5 g/24 h/below pH 1	stirring at 70 °C for 10 h, $KClO_3$, HCl, DI water	30
PB active pharmaceutical ingredient	715	0.1 g/24 h/pH 8	commercially obtained	14
commercially available pigment	∼6	0.5 g/6 h/pH 2.5	commercially obtained	10
commercial PB	832	0.002 g/14 h/pH 5.6	commercially obtained	this study
PB_mechano	1260	0.002 g/14 h/pH 5.6	mechanical grinding at RT for 20 min, no additive, no solvent	this study

https://doi.org/10.1021/acsomega.1c05062
ACS Omega 2022, 7, 3222−3229

the efficient, economical, and eco-friendly purification of radioactive wastewater.

■ ASSOCIATED CONTENT

Supporting Information

The Supporting Information is available free of charge at https://pubs.acs.org/doi/10.1021/acsomega.1c05062.

Williamson−Hall plot and Nelson−Riley plot of PB_mechano and commercial PB; photo images and optical reflectance spectra of PB_mechano and commercial PB; color analysis results of PB_mechano and commercial PB; nitrogen adsorption−desorption isotherms of PB_mechano and commercial PB; zeta potential of commercial PB at pH 5.6; and zeta potential of PB_mechano at pH 5.6 (PDF)

■ AUTHOR INFORMATION

Corresponding Author

Seung-Yeop Kwak − *Department of Materials Science and Engineering, Seoul National University, Seoul 08826, South Korea; Research Institute of Advanced Materials (RIAM) and Institute of Engineering Research, Seoul National University, Seoul 08826, South Korea;* orcid.org/0000-0002-8903-4287; Phone: +82-2-880-8365; Email: sykwak@snu.ac.kr; Fax: +82-2-885-1748

Author

Ji Hwan Lee − *Department of Materials Science and Engineering, Seoul National University, Seoul 08826, South Korea*

Complete contact information is available at: https://pubs.acs.org/10.1021/acsomega.1c05062

Notes

The authors declare no competing financial interest.

■ ACKNOWLEDGMENTS

This work was supported by the project for Collabo R&D between Industry, Academy, and Research Institute funded by the Korea Ministry of SMEs and Startups in 2019 (Project no. 0420-20190000) and SNU Materials Education/Research Division for Creative Global Leader (No. 4120200513611).

■ REFERENCES

(1) Majidnia, Z.; Idris, A. Evaluation of Cesium Removal from Radioactive Waste Water Using Maghemite PVA−Alginate Beads. *Chem. Eng. J.* **2015**, *262*, 372−382.

(2) Kim, Y. K.; Bae, K.; Kim, Y.; Harbottle, D.; Lee, J. W. Immobilization of Potassium Copper Hexacyanoferrate in Doubly Crosslinked Magnetic Polymer Bead for Highly Effective Cs^+ Removal and Facile Recovery. *J. Ind. Eng. Chem.* **2018**, *68*, 48−56.

(3) Mihara, Y.; Sikder, M. T.; Yamagishi, H.; Sasaki, T.; Kurasaki, M.; Itoh, S.; Tanaka, S. Adsorption Kinetic Model of Alginate Gel Beads Synthesized Micro Particle-Prussian Blue to Remove Cesium Ions from Water. *J. Water Proc. Eng.* **2016**, *10*, 9−19.

(4) Faustino, P. J.; Brown, A.; Lowry, B.; Yang, Y.; Wang, Y.; Khan, M. A.; Dunbar, K. R.; Mohammad, A. Quantitative Evaluation of the Thallium Binding of Soluble and Insoluble Prussian Blue Hexacyanoferrate Analogs: A Scientific Comparison Based on Their Critical Quality Attributes. *Inter. J. Pharm.* **2019**, *569*, 118600.

(5) Rani, M.; Shanker, U. Effective adsorption and enhanced degradation of various pesticides from aqueous solution by Prussian blue nanorods. *J. Environ. Chem. Eng.* **2018**, *6*, 1512−1521.

(6) Samain, L.; Grandjean, F.; Long, G. J.; Martinetto, P.; Bordet, P.; Strivay, D. Relationship between the Synthesis of Prussian Blue Pigments, Their Color, Physical Properties, and Their Behavior in Paint Layers. *J. Phys. Chem. C* **2013**, *117*, 9693−9712.

(7) Zakaria, M. B.; Chikyow, T. Recent Advances in Prussian Blue and Prussian Blue Analogues: Synthesis and Thermal Treatments. *Coord. Chem. Rev.* **2017**, *352*, 328−345.

(8) Kim, H.; Kim, M.; Lee, W.; Kim, S. Rapid Removal of Radioactive Cesium by Polyacrylonitrile Nanofibers Containing Prussian Blue. *J. Hazard. Mater.* **2018**, *347*, 106−113.

(9) Jang, S.-C.; Kang, S.-M.; Haldorai, Y.; Giribabu, K.; Lee, G.-W.; Lee, Y.-C.; Hyun, M. S.; Han, Y.-K.; Roh, C.; Huh, Y. S. Synergistically Strengthened 3D Micro-Scavenger Cage Adsorbent for Selective Removal of Radioactive Cesium. *Sci. Rep.* **2016**, *6*, 38384.

(10) Ishizaki, M.; Akiba, S.; Ohtani, A.; Hoshi, Y.; Ono, K.; Matsuba, M.; Togashi, T.; Kananizuka, K.; Sakamoto, M.; Takahashi, A.; Kawamoto, T.; Tanaka, H.; Watanabe, M.; Arisaka, M.; Nankawa, T.; Kurihara, M. Proton-Exchange Mechanism of Specific Cs^+ Adsorption via Lattice Defect Sites of Prussian Blue Filled with Coordination and Crystallization Water Molecules. *Dalton Trans.* **2013**, *42*, 16049−16055.

(11) Takahashi, A.; Tanaka, H.; Minami, K.; Noda, K.; Ishizaki, M.; Kurihara, M.; Ogawa, H.; Kawamoto, T. Unveiling Cs-adsorption Mechanism of Prussian Blue Analogs: Cs^+-Percolation via Vacancies to Complete Dehydrated State. *RSC Adv.* **2018**, *8*, 34808−34816.

(12) Fujita, H.; Sasano, H.; Miyajima, R.; Sakoda, A. Adsorption Equilibrium and Kinetics of Cesium onto Insoluble Prussian Blue Synthesized by an Immediate Precipitation Reaction between Fe^{3+} and $[Fe(CN)_6]^{4-}$. *Adsorption* **2014**, *20*, 905−915.

(13) Yang, H.-M.; Hwang, J. R.; Lee, D. Y.; Kim, K. B.; Park, C. W.; Kim, H. R.; Lee, K.-W. Eco-Friendly One-Pot Synthesis of Prussian Blue-Embedded Magnetic Hydrogel Beads for the Removal of Cesium from Water. *Sci. Rep.* **2018**, *8*, 11476.

(14) Faustino, P. J.; Yang, Y.; Progar, J. J.; Brownell, C. R.; Sadrieh, N.; May, J. C.; Leutzinger, E.; Place, D. A.; Duffy, E. P.; Houn, F.; Loewke, S. A.; Mecozzi, V. J.; Ellison, C. D.; Khan, M. A.; Hussain, A. S.; Lyon, R. C. Quantitative Determination of Cesium Binding to Ferric Hexacyanoferrate: Prussian Blue. *J. Pharm. Biomed. Anal.* **2008**, *47*, 114−125.

(15) Canivet, J.; Vandichel, M.; Farrusseng, D. Origin of Highly Active Metal-Organic Framework Catalysts: Defects? Defects. *Dalton Trans.* **2016**, *45*, 4090−4099.

(16) Fang, Z.; Bueken, B.; De Vos, D. E.; Fischer, R. A. Defect-Engineered Metal-Organic Frameworks. *Angew. Chem., Int. Ed. Engl.* **2015**, *54*, 7234−7254.

(17) Ren, J.; Ledwaba, M.; Musyoka, N. M.; Langmi, H. W.; Mathe, M.; Liao, S.; Pang, W. Structural Defects in Metal−Organic Frameworks (MOFs): Formation, Detection and Control towards Practices of Interests. *Coord. Chem. Rev.* **2017**, *349*, 169−197.

(18) Ralphs, K.; Hardacre, C.; James, S. L. Application of Heterogeneous Catalysts Prepared by Mechanochemical Synthesis. *Chem. Soc. Rev.* **2013**, *42*, 7701−7718.

(19) Boldyreva, E. Mechanochemistry of Inorganic and Organic Systems: What is Similar, What is Different? *Chem. Soc. Rev.* **2013**, *42*, 7719−7738.

(20) Štrukil, V.; Fabian, L.; Reid, D. G.; Duer, M. J.; Jackson, G. J.; Eckert-Maksic, M.; Friscic, T. Towards an Environmentally-Friendly Laboratory: Dimensionality and Reactivity in the Mechanosynthesis of Metal-Organic Compounds. *Chem. Commun.* **2010**, *46*, 9191−9193.

(21) Lee, I.; Kim, S.-H.; Rethinasabapathy, M.; Haldorai, Y.; Lee, G.-W.; Choe, S. R.; Jang, S.-C.; Kang, S.-M.; Han, Y.-K.; Roh, C.; Cho, W.-S.; Huh, Y. S. Porous 3D Prussian Blue/Cellulose Aerogel as a Decorporation Agent for Removal of Ingested Cesium from the Gastrointestinal Tract. *Sci. Rep.* **2018**, *8*, 4540.

(22) Fujita, H.; Miyajima, R.; Sakoda, A. Limitation of Adsorptive Penetration of Cesium into Prussian Blue Crystallite. *Adsorption* **2015**, *21*, 195−204.

(23) Pal, U.; Pérez-Centeno, A.; Herrera-Zaldívar, M. Cathodoluminescence Defect Characterization of Hydrothermally Grown SnO_2 Nanoparticles. *J. Appl. Phys.* **2008**, *103*, 064301.
(24) Vipin, A. K.; Fugetsu, B.; Sakata, I.; Isogai, A.; Endo, M.; Li, M.; Dresselhaus, M. S. Cellulose Nanofiber Backboned Prussian Blue Nanoparticles as Powerful Adsorbents for the Selective Elimination of Radioactive Cesium. *Sci. Rep.* **2016**, *6*, 37009.
(25) Vincent, T.; Vincent, C.; Barré, Y.; Guari, Y.; Le Saout, G.; Guibal, E. Immobilization of Metal Hexacyanoferrates in Chitin Beads for Cesium Sorption: Synthesis and Characterization. *J. Mater. Chem. A* **2014**, *2*, 10007.
(26) Herren, F.; Fischer, P.; Ludi, A.; Haelg, W. Neutron-Diffraction Study of Prussian Blue, $Fe_4[Fe(CN)_6]_3.xH_2O$ - Location of Water-Molecules and Long-Range Magnetic Order. *Inorg. Chem.* **1980**, *19*, 956−959.
(27) Al-Muhtaseb, A. a. H.; Ibrahim, K. A.; Albadarin, A. B.; Alikhashman, O.; Walker, G. M.; Ahmad, M. N. M. Remediation of Phenol-Contaminated Water by Adsorption Using Poly(Methyl Methacrylate) (PMMA). *Chem. Eng. J.* **2011**, *168*, 691−699.
(28) Lee, J. H.; Kwak, S.-Y. Rapid Adsorption of Bisphenol A from Wastewater by β-Cyclodextrin-Functionalized Mesoporous Magnetic Clusters. *Appl. Surf. Sci.* **2019**, *467*−*468*, 178−184.
(29) Zampardi, G.; Sokolov, S. V.; Batchelor-McAuley, C.; Compton, R. G. Potassium (De-)insertion Processes in Prussian Blue Particles: Ensemble versus Single Nanoparticle Behaviour. *Chem.—Eur. J.* **2017**, *23*, 14338−14344.
(30) Taj, S.; Muhammad, D.; Chaudhry, M. A.; Mazhar, M. Lithium, Rubidium and Cesium Ion Removal Using Potassium Iron(III) Hexacyanoferrate(II) Supported on Polymethylmethacrylate. *J. Radioanal. Nucl. Chem.* **2010**, *288*, 79−88.

https://doi.org/10.1021/acsomega.1c05062
ACS Omega 2022, 7, 3222−3229